

ENHANCED LENSING RATE BY CLUSTERING OF MASSIVE GALAXIES: NEWLY DISCOVERED SYSTEMS IN THE SLACS FIELDS

ELISABETH R. NEWTON¹, PHILIP J. MARSHALL¹, AND TOMMASO TREU^{1,2}

Draft version November 3, 2018

ABSTRACT

Galaxy-scale strong gravitational lens systems are useful for a variety of astrophysical applications. However, their use is limited by the relatively small samples of lenses known to date. It is thus important to develop efficient ways to discover new systems both in present and forthcoming datasets. For future large high-resolution imaging surveys we anticipate an ever-growing need for efficiency and for independence from spectroscopic data. In this paper, we exploit the clustering of massive galaxies to perform a high efficiency imaging search for gravitational lenses. Our dataset comprises 44 fields imaged by the Hubble Space Telescope (HST) Advanced Camera for Surveys (ACS), each of which is centered on a lens discovered by the Strong Lens ACS Survey (SLACS). We compare four different search methods: 1) automated detection with the HST Archive Galaxy-scale Gravitational Lens Survey (HAGGLEs) robot, 2) examining cutout images of bright galaxies (BGs) after subtraction of a smooth galaxy light distribution, 3) examining the unsubtracted BG cutouts, and 4) performing a full-frame visual inspection of the ACS images. We compute purity and completeness and consider investigator time for the four algorithms, using the main SLACS lenses as a testbed. The first and second algorithms perform the best. We present the four new lens systems discovered during this comprehensive search, as well as one other likely candidate. For each new lens we use the fundamental plane to estimate the lens velocity dispersion and predict, from the resulting lens geometry, the redshifts of the lensed sources. Two of these new systems are found in galaxy clusters, which include the SLACS lenses in the two respective fields. Overall we find that the enhanced lens abundance (30^{+24}_{-8} lenses/degree²) is higher than expected for random fields (12^{+4}_{-2} lenses/degree² for the COSMOS survey). Additionally, we find that the gravitational lenses we detect are qualitatively different from those in the parent SLACS sample: this imaging survey is largely probing higher-redshift, and lower-mass, early-type galaxies.

Subject headings: gravitational lensing – techniques: miscellaneous – surveys

1. INTRODUCTION

Strong gravitational lensing – when the potential of a massive foreground object causes the formation of multiple images of a background source – is a powerful tool for cosmological and astrophysical research. Applications include measuring the mass distributions of dark and luminous matter, and measuring cosmological parameters via the lens geometry or abundance (see e.g. Kochanek 2006, for a review). A homogenous, well-understood sample of lenses is required for a statistically significant study, necessitating large-scale, systematic surveys (Turner et al. 1984; Bolton et al. 2006; Inada et al. 2008). The ~ 200 galaxy-scale lenses known today have been found through the numerous selection algorithms described in the next paragraph, and include a significant number of serendipitous discoveries. Although this has enabled substantial progress, the number is still the limiting factor for many applications.

Most searches so far have focused on either the source or lens population, employing a range of different strategies. Searches targeting potential sources have included looking for multiply-imaged radio sources – as in the Cosmic Lens All-Sky Survey (CLASS; Myers et al. 2003; Browne et al. 2003) – and examining known quasars (e.g.

Maoz et al. 1997; Pindor et al. 2003). The Sloan Digital Sky Survey (SDSS) Quasar Lens Search (Oguri et al. 2006; Inada et al. 2008) selects lensed quasar candidates using two algorithms, one based on morphology and color for small-separation images, and one based only on color. Of the surveys targeting potential lenses, most have involved inspection of high resolution images. Ratnatunga et al. (1999) and Moustakas et al. (2007) selected candidates by eye from HST color images of the Extended Groth Strip (EGS) fields. Other authors have attempted to pre-select massive galaxies by their optical magnitude and color, and then examine the residuals after galaxy subtraction. This was done in the Great Observatories Origins Deep Survey (GOODS) lens search (Fassnacht et al. 2004) and the Cosmic Evolution Survey (COSMOS) lens search (Faure et al. 2008). Most recently, Jackson (2008) extended this method to lower mass galaxies, but focused on viewing large-format arrays of unsubtracted color galaxy cutout images. The Sloan Lens ACS Survey (Bolton et al. 2006, 2008a) candidates were selected based on spectroscopic data indicating multiple redshifts in the spectrum of early-type (and hence massive) galaxies, then classified using this data and visual examination of high resolution HST images (before and after lens galaxy subtraction).

Recently, several algorithms for automated lens detection have been developed. Those developed by Alard (2006), Seidel & Bartelmann (2007) and

¹ Department of Physics, University of California, Santa Barbara, CA 93106-9530

² Alfred P. Sloan Research Fellow; Packard Fellow

Kubo & Dell’Antonio (2008) look for arcs, a common feature in both weak and strong lensing on group and cluster scales. Estrada et al. (2007) and Belokurov et al. (2007) suggest mining databases for blue objects near potential lenses, since the most common sources are faint blue background galaxies. The RingFinder (Cabanac et al. 2007) applies the same logic to smaller image separation lenses, subtracting a rescaled red image from a blue cutout image to dig within the lens light distribution; it then analyzes the shapes and positions of the remaining residuals. Most recently the HAGGLEs automated lens detection “robot” (Marshall et al. 2008) attempts to model every object (typically selected to be Bright Red Galaxies or BRGs) as a gravitational lens, i.e. as a combination of background light from the source that is consistent with having been multiply-imaged, and residual foreground light from the lens galaxy. The result is the robot’s quantitative prediction of how a human would have classified the candidate.

Fortunately, we are about to enter an era when orders of magnitude increases in the number of known lenses will be possible. In the near future, wide-field surveys such as the proposed Joint Dark Energy Mission (JDEM) and Euclid space missions would provide $\sim 10^3 - 10^4$ square degrees of high resolution imaging data (Marshall et al. 2008). Automation will be needed to examine such large areas over manageable timescales, and to draw attention to those systems which have a higher probability of being lenses. We also must be prepared to proceed without the help of spectroscopic data.

We describe here just such a survey: based purely on imaging data, and with a sufficient degree of automation. We compare the accuracy of four methods of searching for strong gravitational lenses. Presented in order of degree of automation, they are: (1) using the HAGGLEs robot (Marshall et al. 2008), (2) examining subtraction residuals (e.g. Faure et al. 2008), (3) looking at galaxy cutouts (e.g. Fassnacht et al. 2004; Jackson 2008), and (4) performing a visual inspection of entire fields (e.g. Moustakas et al. 2007).

We additionally aim to make use of galaxy clustering in order to improve the efficiency of our search, as suggested by Fassnacht et al. (2006). The most likely lensing galaxies are massive ellipticals with $0.3 < z < 1.3$ (Turner et al. 1984; Fassnacht et al. 2004): we may expect that focusing on bright red galaxies (BRGs) will increase the lens detection efficiency (e.g. Fassnacht et al. 2004; Faure et al. 2008; Marshall et al. 2008). The sources, meanwhile, are predominantly expected to be faint blue galaxies (FBGs) at redshifts at or above 1 (Marshall et al. 2005). Both of these types of objects (potential lenses and potential sources) are clustered, BRGs more strongly than FBGs. We therefore expect that strong gravitational lenses are also clustered; we anticipate finding more new lenses by looking near known ones than we would otherwise. For example, Fassnacht et al. (2006) presents just such an occurrence: the researchers discovered two additional lens candidates less than 40 arc-sec from the known lens B1608+656.

Therefore, as our dataset we use a subset of the SLACS HST/ACS fields. The SLACS survey has discovered 70 definite galaxy-galaxy strong lenses (Bolton et al. 2008a) to date. These definite lenses have clearly identifiable

lenses arcs or multiple images in addition to spectroscopic data; due to the rigorous requirements for this classification, we consider all to be confirmed lenses. Of these, 63 are well-modeled by a singular isothermal ellipsoid (SIE) and have lens and source redshifts along with F814W photometry for the lens galaxy; most also have measured stellar velocity dispersions (Bolton et al. 2008a). This makes the SLACS lenses the largest homogenous sample of strong lenses to date. Each of the fields we use is centered on one of the known SLACS lenses (hereafter the “main lens”); we thus make use of gravitational lens clustering in every field. The majority of our fields were observed in just one filter, meaning that we by necessity pre-select bright galaxies (BGs) rather than BRGs. For the automated portion of our searches, we use the HAGGLEs robot which, in addition to performing a quantitative lens classification, creates a useful database of galaxy cutouts and residuals.

The organization of this paper is as follows. In Section 2 we present the 44 ACS fields in our dataset, and in Section 3 we outline the four search procedures we used to find gravitational lenses in these images. To assess the accuracy of these methods, we discuss each procedure’s performance on the main lenses in Section 4. We then present our four new definite strong lensing systems and one likely candidate, and investigate their physical properties and environments, in Section 5. After some discussion of our methods and results in Section 6, we conclude in Section 7. All magnitudes are in the AB system; we assume a flat cosmology with $\Omega_m=0.3$, $\Omega_\Lambda=0.7$, and $H_0=100h$ kms $^{-1}$ Mpc $^{-1}$, where $h=0.7$ when necessary.

2. SAMPLE SELECTION AND OBJECT DETECTION

We use a subsample of the ACS F814W fields investigated in the Sloan Lens ACS Survey (SLACS; Bolton et al. 2006; Treu et al. 2006; Koopmans et al. 2006; Gavazzi et al. 2007; Bolton et al. 2008a; Gavazzi et al. 2008; Bolton et al. 2008b; Treu et al. 2008), hereafter papers SLACS-I through VIII. The sample selection and data reduction and analysis of the SLACS data is given in SLACS-I, -IV and -V and will not be repeated here. We select the subset of 44 definite lenses whose ACS observations meet the following two requirements: exposure time >1000 seconds through F814W, and lens classification “definite.” Due to the demise of ACS, two filters are not available across all fields; of the ACS filters used, F814W is the most widely available in the SLACS fields. 14 fields were additionally imaged through F555W. We require long exposure time to guarantee the ability to produce deep, high quality, cosmic ray-free reduced images.

Our final sample comprises 44 uniformly-observed ACS fields, each centered on a SLACS gravitational lens (a “main lens”). Each field covers approximately 11 arcmin 2 ; thus our total survey area is 0.134 square degrees.

Most lens-finding methods involve examining bright galaxies (BGs), as being the most likely to be lensing galaxies (e.g. Fassnacht et al. 2004; Faure et al. 2008; Marshall et al. 2008). Here this selection is done with magnitude and size cuts on catalogs made with the SEX-

tractor³ software tool; only a third of our fields have multi-filter ACS data so in order to maintain consistency we do not use color selection even when it is possible. We choose an apparent F814W magnitude (m_{F814W} ; using Kron-like elliptical apertures) limit of 22. Other limits were tried, but 22 was found empirically to be the best balance between efficiency and the selection of all bright galaxies: with $m_{F814W} < 22$, a total of 2399 BGs are selected, but with $m_{F814W} < 23$, that number jumps to 5439 without adding significantly to the actual number of morphologically early-type galaxies selected. The minimum size selected is FWHM=0".215, in order to reject most stars. We additionally use the SExtractor “flags” parameter to limit the remaining contaminants.

3. SEARCH METHODS

We use four distinct methods to search for gravitational lenses. They are presented in order of degree of automation, where the first has the most pre-selection and analysis, and the last none:

- Procedure 1: Using output from the HAGGLEs robot
- Procedure 2: Inspection of subtraction residuals of bright galaxies
- Procedure 3: Inspection of cutout images of bright galaxies
- Procedure 4: Full-frame visual inspection of the ACS images

In general we expect our searches to be sensitive to lensing events similar to, but fainter than, the SLACS main lenses. With the BG selection in Procedures 1–3, and the innate limits of the human eye in Procedure 4, we are biased towards lensing events around large, luminous galaxies. However, empirically the main lenses are the brightest objects (other than saturated stars) in the fields, so we expect any other lenses we find to be, by necessity, fainter. The main lenses also favor high magnification configurations (Einstein rings) due presumably to their spectroscopic selection; we expect to be somewhat preferential in this regard as well, on the grounds that these distinctive cases will be easiest to identify visually.

Before continuing, we first consider the question “what is the probability that this object is a gravitational lens?” The classification of lens candidates has varied among the major surveys targeting potential lenses, as has the data on which these classifications are based. The COSMOS lens search (Faure et al. 2008) sample is subdivided into “best systems”, which are deemed to have a greater probability of being lenses than the remaining objects. GOODS (Fassnacht et al. 2004) selected candidates and voted to choose “top candidates.” Jackson (2008) groups potential lenses into three categories: very likely or certain lenses, possible or probable lenses, and not-lenses. The SLACS survey (Bolton et al. 2008a) also groups candidates into three categories (definite lenses, probable lenses, and inconclusive/not lenses). We note that the classification of definite or probable lenses is not the same across surveys, and therefore one has to be careful to

TABLE 1
LENS CLASSIFICATION SYSTEMS

Human class H	Robot class H_r	Definition
3	>2.5	Definitely a lens
2	1.5 to 2.5	Probably a lens
1	0.5 to 1.5	Possibly a lens
0	<0.5	Definitely not a lens

impose similar quality criteria when comparing inferred density of lens galaxies.

In this work we follow Marshall et al. (2008) and employ a 4-point subjective classification scheme, outlined in Table 1: the classification parameter H may range from 3 (definite lenses), through 2 (probable lenses) and 1 (possible lenses), to $H = 0$ (definitely not lenses). Each of the 44 fields in our sample contains a confirmed lens from the SLACS survey, where here the grade is based on all available data, notably the galaxy spectrum (including anomalous high redshift emission lines) and clear lensing-consistent residuals after lens galaxy light subtraction in all procured filters. We thus assign the classification parameter $H = 3$ for each main lens.

Humans (after some training) are adept at identifying gravitational lenses by eye, using high resolution imaging data alone; we effectively make an internal model for the lens and optimize it. However, the amount of information available during each lens search with which to do this may vary: in any given search we always lack additional understanding that would aid us in identifying lenses. When carrying out the four different search procedures, we therefore assign each system a value H_i (where $i = 1, 2, 3$ or 4): each of these is our best guess as to the classification that a trained human would have assigned the system, if they had been given only the data presented in the i^{th} procedure. (This results in four “re-classifications” for each main lens.) We consider the “true” classification H to be the value we give an object when taking into account *all data*.

3.1. Procedure 1: HAGGLEs robot

In Procedure 1, we use the HAGGLEs robot, the automated lens detection program developed by Marshall et al. (2008), to identify samples of lens candidates prior to visual inspection. The robot treats every object as if it were a lens, models it, and then calculates how well the lens hypothesis works. It extracts and uses 6 arc-second square cutout images of each object, and then focuses on the residuals made by subtracting off an elliptically symmetric Moffat profile model for the putative lens galaxy light. The gravitational potential of the lensing galaxy is assumed to be sufficiently well-described by a singular isothermal sphere (SIS) plus external shear; this model is fitted to the residual image. Disk-like features and bright neighboring objects are masked before fitting. When multi-filter data is available it is used, and although the robot does not rely on color, with its performance is expected to improve (Marshall et al. 2008). Based on the results of the modeling process, the robot calculates and assigns a value of H_r to each object, where H_r is the robot’s estimate of the classification H a human would have given the system. We summarize the human and robot classifications in Table 1 (after Marshall et al.

³ <http://terapix.iap.fr/>

TABLE 2
PRIOR PROBABILITY DISTRIBUTIONS FOR ROBOT CHARACTERS

Character	$\Pr(H=0)$	$\Pr(H=1)$	$\Pr(H=2)$	$\Pr(H=3)$
Realistic	0.900	0.080	0.019	0.001
Optimistic	0.050	0.100	0.250	0.600

2008).

The robot may have one of two characters, reflecting the prior probability that an object is a lens. The “realistic” character robot might expect 0.1% of objects to be lenses, and the “optimistic” character robot might expect 60% to be (Marshall et al. 2008). The realistic robot is approximately in accordance with current estimates of the fraction of strongly lensed galaxies (e.g. Bolton et al. 2006; Moustakas et al. 2007; Marshall et al. 2008), while the optimistic robot has the advantage of being most inclusive by giving higher values of H_r . These two prior probability distributions are given in Table 2 (after Marshall et al. 2008). Marshall et al. (2008) note that while the realistic robot produces lens samples of high purity – and correspondingly little need for human inspection – a highly complete search requires, at present, a more optimistic robot.

We ran both the optimistic and realistic robots in order to verify this last claim, but chose to use the optimistic robot to search for new lenses, as our sample is small and we are most interested in finding all lenses present in our sample. When comparing the performances of both robots, we refer to the optimistic and realistic robot classifications as H_r^{opt} and H_r^{real} , respectively. The main goal of the comparison is to gain insight into the populations of objects selected, and thus help improve the automated part of this procedure for future surveys.

The output from the robot includes an individualized webpage for each object, containing the cutout, subtraction residual, masked residual, and estimation of Einstein radius. This page also displays the minimal source able to produce the observed configuration, and the predicted image-plane residual reconstructed from this minimal source (see Marshall et al. 2008, for more details). We viewed the pages of objects for which $H_r^{opt} > 1.5$ (indicating optimistically probable and definite lenses), and gave each object a human classification H_1 , using the same data that was available to the robot (namely, the cutout image and subtraction residual image), and the lensmodel outputs produced by the robot.

3.2. Procedure 2: Examining BG residuals

Procedure 2 makes use only of the subtraction residuals produced by the robot. We examine the residuals of every BG initially selected in the fields; all of the 6'' by 6'' subtraction residual cutouts for a field are displayed in a grid for rapid viewing. When multi-filter data is available, the residuals are shown in color. Looking at the 44 grids, we note all objects of interest; to each of these objects we assign a human classification H_2 , based solely on the subtraction residual data.

3.3. Procedure 3: Examining BG cutouts

In this method, we inspect each of the 6'' by 6'' cutouts of the BGs provided by the HAGGLeS robot. We again

display the cutout images in a grid for rapid viewing, making this procedure very similar to that employed by Jackson (2008). However, the stretch of the cutouts’ image display is fixed for all objects at a level appropriate to the EGS-type lenses (Moustakas et al. 2007). This makes this method particularly sensitive to faint lensing events, and somewhat insensitive to lensing by very bright galaxies. We assign objects of interest a human classification, this time H_3 , using only the galaxy cutout on display.

3.4. Procedure 4: Full-frame visual inspection

During the full-frame visual inspection, each of the 44 fields’ F814W ACS images is viewed with ds9.⁴ We initially set image parameters in each field so as to be sensitive to the lensing events we expect to find: similar to, but fainter than, the main lenses. We do this by setting the intensity stretch such that the main lens is slightly over-saturated; from this display we select objects of interest. For each object, we adjust the scale limits and intensity stretch such that the potential lensing features are most apparent, then decide on a classification. Procedure 4 differs from the previous three most notably in that all galaxies in the field – not just BGs – are examined, and that their viewing parameters are set individually. The human classification parameter assigned in this procedure is denoted H_4 .

3.5. Summary of Results

During each procedure, any potential gravitational lens was marked and assigned a human classification based only on the information available during the search procedure by which it was found. Following the completion of all searches, all available information was considered holistically and objects were assigned a final human classification H . The classification is based primarily on our ability to recognize a typical lens geometry in the observed morphology (in both the cutout and subtraction residual), on colors and surface brightnesses consistent with lensing, and on the robot’s ability to model the object. In total we discovered four new objects with $H = 3$, and one object with $H = 2$. These new gravitational lenses are presented in Section 5.

4. METHOD ACCURACY

Before investigating the properties of our newly-discovered lenses, we first discuss the performance of the four search procedures in terms of both their ability to find SLACS-type lenses (low redshift, high magnification), and their contribution to the finding of the new gravitational lens systems. For each method, we calculate the purity and completeness of the samples selected, considering our five best systems and the SLACS main lenses together as lens systems to be recovered. We define purity as the percent of selected objects (i.e. having classification parameter H_i above some threshold), that actually have final human classification H greater than the same threshold. Only the SLACS main lenses and our 5 best systems have $H > 1.5$, and all but one of these has $H = 3$. Similarly, completeness is defined as the percent of the objects with final human class H

⁴ <http://hea-www.harvard.edu/RD/ds9/>

TABLE 3
 PURITY AND COMPLETENESS FOR EACH METHOD

Procedure	H_i cut	Purity(%)	Completeness(%)
1	$H_1 > 2.5$	100	69
	$H_1 > 1.5$	100	80
2	$H_2 > 2.5$	100	77
	$H_2 > 1.5$	100	90
3	$H_3 > 2.5$	100	4
	$H_3 > 1.5$	93	22
4	$H_4 > 2.5$	100	81
	$H_4 > 1.5$	100	92
Rea. robot	$H_r^{real} > 2.5$	40	8
	$H_r^{real} > 1.5$	8	41
Opt. robot	$H_r^{opt} > 2.5$	5	27
	$H_r^{opt} > 1.5$	3	82

greater than some threshold that were given procedure classification H_i greater than the same threshold. For Procedure 1, any object that was not examined because $H_r^{opt} < 1.5$ is considered to have $H_1 = 0$. Purity and completeness were calculated for each procedure, and for both the realistic and optimistic robots. These statistics are summarized in Table 3; errors are of order a few percent.

Note that during each search procedure, the main SLACS lenses themselves are classified, resulting in values of H_1 , H_2 , H_3 , and H_4 for each. A lens-by-lens comparison of classification values is available in the Appendix, while data on the total numbers of main lenses and new lens recovered by each search procedure are presented in Table 4. In this table we also include the amount of time spent per field for each method, and include the performance of the HAGGLEs robot (with no human inspection) for comparison.

In the subsections that follow, we briefly discuss these results and their implications for optimizing lens discovery in high resolution imaging surveys. In the Appendix we show, for reference, some of the images that comprise the input data to the first three search procedures, namely, cutout images of the main lenses, and of the $H_r^{real} > 2.5$ candidates.

4.1. Procedure 1

Inspecting all objects classified by the optimistic robot as $H_r^{opt} > 1.5$, we classified three out of the five new systems as $H_1 = 3$, and one system as $H_1 = 2$. The final system had been assigned a robot classification parameter of $H_r^{opt} < 1.5$ and so was not examined. This failure is most likely due to the non-lensed light remaining after the Moffat subtraction (see the Appendix for more illustration of this).

Indeed, for the main lenses, we found that the unmasked disk features are the most common cause of robot detection failures: we show the subtraction residuals and reconstructed images in the Appendix. The robot may fail to find a suitable model entirely in some extreme cases, such as when considering objects with very strong disk components or bright companion galaxies (main lenses SDSSJ1029+0420, SDSSJ1103+5322 and SDSSJ1416+5136). We find overall that 8 of the main lenses, including the three cases just mentioned, are not detected at $H_r^{opt} > 1.5$ by the robot. Interestingly, one of the 36 robot-detected systems, and three of the 8 robot-rejected systems were human-classified

as $H_1 < 1.5$: given just the output from the robot, these lenses (SDSSJ1213+6708, and SDSSJ1016+3859 SDSSJ1029+0420, and SDSSJ1032+5322) would not have been identified as lenses by a human inspector.

The lens galaxy subtraction also seems to be the major cause of false detections: ring-like and disk-like features left over from the Moffat profile subtraction and then incompletely masked can be wrongly interpreted by the robot as lenses. Examples of such false positives can be seen in the 10 objects classified by the realistic robot as $H_r^{real} > 1.5$ (in the Appendix).

Of the 36 robot-detected main lenses, only 20 were classified by the optimistic robot as “definite lenses” ($H_r^{opt} > 2.5$). The reasons for these mis-classifications are a little more subtle. The probability density functions (PDFs) used to calculate the H_r values for this research were determined by Marshall et al. (2008) based on a training set of EGS non-lenses and simulated lenses. By overlaying the robot model output for the SLACS main lenses on these PDFs, we can gain insight into the cause of the robot’s mis-classifications. In Figure 1 we show $\Pr(\mathbf{d}|H = 3)$, and overlay the \mathbf{d} -values for the main lenses (larger data points). Here we clearly see that the PDF (contours approximating the density of smaller, training set points) is not optimized for SLACS-type (low redshift, high magnification) lenses: to the robot, source magnitudes are surprisingly bright and arcs are of unusual thickness. These differences are to be expected, but we note that the lenses we should expect to find with the HAGGLEs robot would therefore be more similar to the EGS lenses in terms of apparent magnitude and geometric configuration. In a future wide-field search, where more SLACS-type lenses may be present, it would be prudent to retrain the robot on a wider variety of lenses – and perhaps on the SLACS sample itself.

Having detected a SLACS main lens, how accurately does the HAGGLEs robot model it? As an illustration of the robotic models’ performance, we compare the robot-calculated Einstein radii (θ_E) to those determined in the SLACS papers (Figure 2). The 12 open data points are main lenses that were not well-modeled by the robot; after removing these we find an rms scatter of 12%. For 60% of the main lenses, then, the robot finds not only a successful lens model, but one that is in very good quantitative agreement with that inferred during the SLACS project.

4.2. Procedure 2

When examining the BG subtraction residual images, we classified all four of the new $H = 3$ systems as $H_2 > 1.5$ or above; the $H = 2$ system was missed. Einstein rings are particularly easy to identify, resulting in a high proportion of the main lenses found. However, we occasionally lost some image context: some residuals are more easily identified as being caused by lensing when viewed along side of the lens galaxy cutout. When looking at both cutouts and subtraction residuals, we are able to ask the question “Is this structure a part of the lensing galaxy or is it unique?” However, since sources are typically bluer than the lens galaxy, color residuals can aid us in answering this question: we note that all but one main lens was classified as $H_2 = 3$ when multiple filters were available.

TABLE 4
SUMMARY OF RESULTS FOR EACH METHOD

Procedure	Rea. robot	Opt. robot	1	2	3	4
Main lenses $H_i > 1.5$	20	36	35	39	8	42
Main lenses $H_i > 2.5$	4	10	30	34	2	36
New lenses $H_i > 1.5$	0	4	4	5	3	3
New lenses $H_i > 2.5$	0	3	3	3	0	3
Typical candidates			arcs multiple images	spirals, arcs multiple images	blue images companions	spirals, arcs companions
Time per field (min)			2-4	1-2	1-2	20-40
Time per degree ² (hours)			10-20	5-10	5-10	100-200

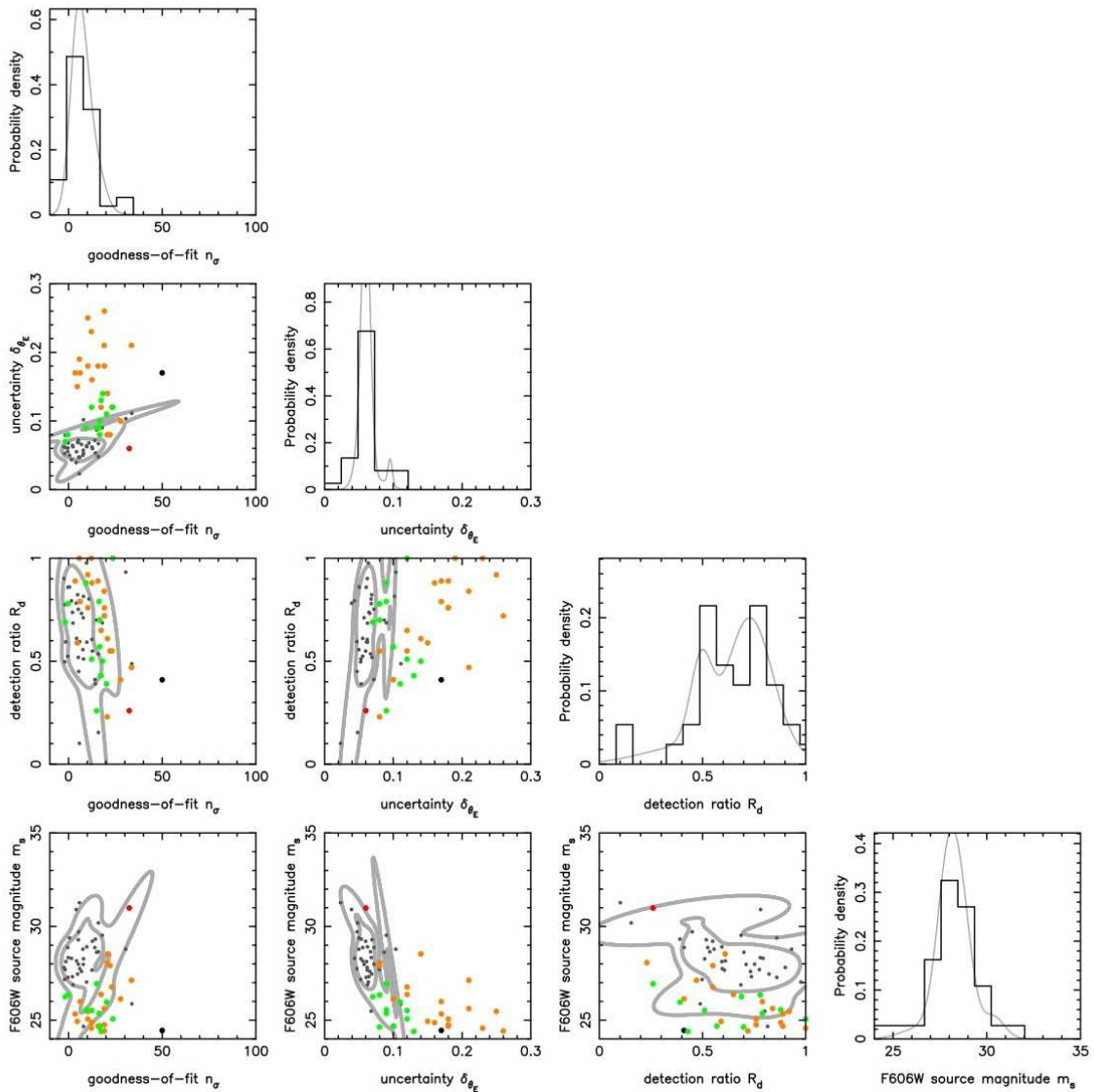


FIG. 1.— $\Pr(d|H=3)$ derived from the robot outputs of the EGS training set (smaller points), overlain with the outputs of the SLACS main lenses (larger points). Points correspond to objects with $H_1=3$ and the contours in this and the subsequent two figures are 68% and 95% CL.. After Marshall et al. (2008).

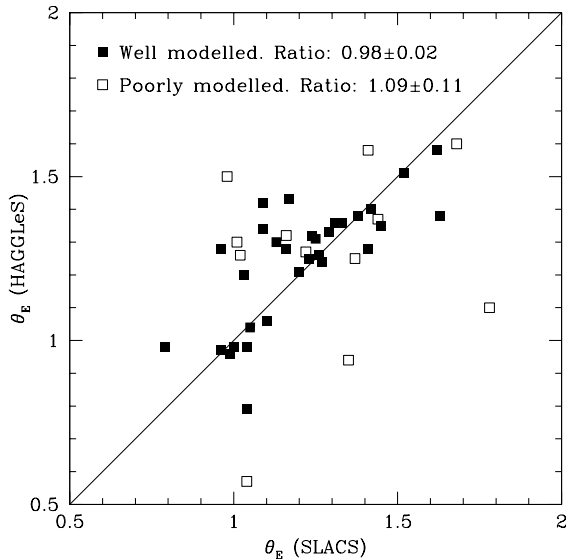


FIG. 2.— Comparison between the SLACS-measured Einstein radii (SLACS-V) and those calculated by the HAGGLeS robot. The systems for which robotic lens modeling failed are represented by filled points. The one-to-one relation is also shown to guide the eye; we find an rms scatter of 12%. Errors on SLACS Einstein Radii are 2% (SLACS-V).

4.3. Procedure 3

We found that Procedure 3 was not an appropriate method to use when looking for occurrences like the SLACS lenses. This is predominantly an issue of image intensity scale and dynamic range. The scales used by the robot are set for fainter lens galaxies than those in the SLACS sample, and as such the main lenses often appear saturated: the lensed features were completely washed out in all but 8 cases. We consequently classified only two objects as $H_3 = 3$, and this is the only procedure in which we falsely identified an object as a lens. This procedure was found to be most effective when lensed images are blue against a red galaxy: five of the eight main lenses given $H_3 > 1.5$ were in color fields. The issue of intensity scaling was noted by Jackson (2008), who attempted to optimize the intensity scale on an object by object basis, and hence performed rather better in terms of “true” lenses recovered (Jackson recovered $\sim 50\%$ of the lenses identified by Faure et al. 2008). However, the large dynamic range in surface brightness of the lens and source galaxies makes this a very difficult task.

4.4. Procedure 4

In Procedure 4 we found three out of four new $H = 3$ lenses, and only two of the main lenses were not classified as $H_4 > 1.5$. The greatest strength of this method lies in the ability to vary the intensity scale of the image so as to make apparent any lensed structures. It is effectively the same as looking at both a cutout and a subtraction residual: lensing can be viewed in the context of the host galaxy. Its weaknesses, however, are in the time required and the quantity of data presented: it is difficult to conduct a thorough, mistake-free search when every object must be examined and the time required is ~ 30 minutes per field.

4.5. Considerations and comparisons

We find that procedures one and two are nearly identical in their ability to find new lenses, while the latter performed marginally better on the main lenses since all the objects were examined. Procedure 3 we find unsuited to the task at hand; looking at the robot output (Procedure 1) or subtraction residuals (Procedure 2) largely circumvents the dynamic range problems of image display, and produces superior results. Procedure 4 is the most inclusive of the four procedures as all galaxies (not just bright galaxies) are examined; it is also the only procedure in which we would have a chance of finding a “dark lens.” However, we found two additional lensing systems when we pre-selected bright galaxies and our search took significantly less time. We hence find that looking only at the BG subsample does not decrease the completeness of a survey, and could in fact improve it due to a lower error-rate.

Taking into consideration efficiency, completeness, and purity, we recommend the use of Procedure 1 and Procedure 2. There will be cases, such as with eight of the main lenses and one of our new lenses, where a lens will be missed by the current robot and thus by the human following Procedure 1. There are also certain lenses, particularly very unusual ones, that the current robot will miss due to its inability to model it. For example, the naked cusp configuration that often occurs with edge-on spirals produces three images blended into an arc but no counter-image; without a counter image the current robot will classify the system as a class 0. Additionally, when the environment plays a strong role – in over-dense environments for instance – the simple SIS+external shear model used now may not be sufficient. It therefore may be preferential to use a combination of procedures 1 and 2, inspecting *all* objects modeled by the robot regardless of the modeling outcome.

5. RESULTS

We have discovered four new definite gravitational lenses and one promising lens candidate. These five systems were each found in at least one of the four separate search procedures. Having taken into consideration all available data—including spectroscopy for one system—we assigned four objects true human classification $H = 3$ (our four new lenses), and only one $H = 2$ (our best candidate). The five systems were also classified during each of the procedures. Classifications for potential lenses are referred to as H_1 , H_2 , H_3 , or H_4 according to procedure number; these values may differ from H . We present the systems along with their classifications in Table 5. For simplicity, each lens is given a short name that will be used in the remainder of this paper.

5.1. Improved Robotic Lens Models

As shown in Section 4, and noted by Marshall et al. (2008), the lens model parameters returned by the HAGGLeS robot are not always accurate. We find that the principal cause of robot modeling (and indeed classification) error is insufficient lens light subtraction. Disks and irregular profile slopes both give rise to significant symmetrical residuals that confuse the robot. For the small number of high quality lens candidates identified in section 5, we can solve this problem on a case by case basis, and provide the robot with cleaner images to model, and

TABLE 5
CLASSIFICATION OF NEW CANDIDATES BY METHOD

Short name	Object name	H	H ₁	H ₂	H ₃	H ₄	H _r ^{real}	H _r ^{opt}
Danny	HST J073736.40+321540.3	3	3	3	2	3	0.9	1.9
Frenchie	HST J114331.46−014508.0	3	0 ^a	2	2	0	0.1	1.1
Kenickie	HST J121346.57+670833.3	3	3	3	2	3	0.7	2.9
Sandy	HST J143001.28+410440.8	3	3	3	1	3	0.2	2.9
Rizzo	HST J110307.14+532042.6	2	2	2	1	0	0.5	2.7

^a Frenchie was not examined during procedure 1 because $H_r^{opt} < 1.5$ for this system.

thus produce more accurate estimates of the lens candidates’ Einstein radii.

We improved the lens galaxy light subtraction with the flexible B-spline fitting approach developed by Bolton et al. (2006), after first masking out the objects in the image identified as candidate lensed arcs. This procedure leaves sharper lensed image residuals. We then set all undetected pixels to zero as described in Marshall et al. (2008), but also at this stage masked out all the features in the B-spline residual map not identified as lensed arcs. We then re-ran the lens-modeling part of the HAGGLE robot, and took as our final estimated Einstein radius the position of the peak of the Gaussian fit to the source plane flux curve, as described in Marshall et al. (2008). The resulting lens models and their parameters are shown in Figure 3 and Table 6.

We can use our results from Section 4.1 to estimate the accuracy of the Einstein Radii measured by the robot. As shown in Figure 2, we found that – for well modeled lenses – robot- and SLACS-measured Einstein radii agree to within 10%. However, this can be considered an upper limit to our true uncertainty, since we use improved subtractions for the new systems. In practice, the robot’s estimates using improved subtractions are as good as the relatively simple models allow them to be. To be conservative we adopt an error of 5% on the robot’s Einstein Radii.

5.2. Photometry

Available from SDSS¹ are photometric redshifts and apparent lens galaxy magnitudes; with the exception of one (Frenchie), no spectra are available. To supplement the SDSS data, we use the `galfit` software (Peng et al. 2002) to fit de Vaucouleurs models to the Hubble F814W data and derive apparent magnitude and circularized effective radii, listed in Table 6. After correcting for Galactic extinction, we calculate the rest frame V-band magnitude from the observed F814W, a conversion for which there is very little scatter between different spectral types. Details on surface photometry and K-color corrections can be found in the paper by Treu et al. (2001). For the main SLACS lenses we use data from Bolton et al. (2008a).

5.3. Velocity dispersion and source redshift

In this Section we use available spectroscopy and photometry to estimate the velocity dispersion and source redshifts of the new lens systems, using two physically motivated assumptions: i) early-type lens galaxies lie on the fundamental plane (hereafter FP Dressler et al. 1987; Djorgovski & Davis 1987; Treu et al. 2006; Bolton et al.

2008b); ii) the ratio between stellar velocity dispersion and that of the best fitting SIS is approximately constant.

We use the photometric redshift and evolution-corrected V band luminosities to estimate the central stellar velocity dispersion predicted by the FP relation:

$$\log R_e = a \log \sigma_{e,2} + b \log I_e + c, \quad (1)$$

where $\sigma_{e,2}$ is the stellar velocity dispersion corrected to an aperture of radius half the effective radius (in units of 100 km s^{-1}), I_e is the effective surface brightness in units of $10^9 L_\odot \text{ kpc}^{-2}$, and R_e is the effective radius in kpc. We adopt the coefficients $a = 1.28$ $b = -0.77$ $c = -0.09$ derived in SLACS-V for the SLACS sample. The intrinsic scatter of the fundamental plane dominate the uncertainty on the estimated $\sigma_{e,2}$ (0.05 dex). Central stellar velocity dispersions σ_* are obtained from $\sigma_{e,2}$ using the standard correction described in SLACS-V.

Additionally, SLACS-IV and -V found that σ_* is correlated with σ_{SIE} , the velocity dispersion that best fits the model of the lens as a singular isothermal ellipse (SIE). For the SLACS sample:

$$\langle \sigma_* / \sigma_{\text{SIE}} \rangle = 1.02 \pm 0.01. \quad (2)$$

We may also calculate σ_{SIE} , assuming the Einstein radius θ_E , lens redshift, and source redshift are known:

$$\sigma_{\text{SIE}} = c \sqrt{\frac{\theta_E D_s}{4\pi D_{ds}}}, \quad (3)$$

where D_s and D_{ds} are, respectively, angular-diameter distances to the source galaxy and between the lens and source galaxies, and θ_E is given in radians.

We combine Equations 1 to 3 to determine our best estimate of the source redshift. To obtain the posterior probability distribution function of z_s , we assume that σ_* is log-normally distributed with scatter 0.06 dex, which is dominated by the intrinsic scatter of the FP and of Eq 2. We adopt priors appropriate for the source population. For the newly discovered – imaging selected – lenses, we adopt as prior the redshift distribution of faint galaxies in single orbit ACS-F814W data as measured by the COSMOS survey. For the main SLACS lenses we adopt the same prior, but truncated at $z_s < 1.5$, i.e. the highest redshift where [O II] is still visible within the observed wavelength range covered by the SDSS spectrograph used for discovery. The results change very little if a uniform prior is adopted instead.

The result of this calculation for the main lenses can be seen in Figures 4 and 5. The former compares the estimated source redshifts to the known source redshifts for the main SLACS sample. This sanity check indicates

¹ <http://cas.sdss.org/dr6/en/>

TABLE 6
RELEVANT LENSING DATA FOR NEW LENSES

Short name	Separation (arcsec)	θ_E (arcsec)	F814W	R_e (arcsec)	z_d	z_s	σ_* (km s ⁻¹)	$\sigma_{*,FP}$ (km s ⁻¹)	Morphology
Danny	107.9±0.2	0.65±0.03	18.75	0.61	0.34±0.03	0.48 ^{+0.03} _{-0.02}	–	296±41	S0
Main lens		1.00	17.04	2.82	0.3223	0.5812	358±17	313±43	E/S0
Frenchie	46.8±0.2	1.45±0.07	16.10	1.79	0.104	0.91 ^{+0.15} _{-0.56}	248±17	226±31	E
Main lens		1.02	14.96	4.80	0.106	0.4019	279±13	269±37	E/S0
Kenickie	35.2±0.2	0.65±0.03	19.99	0.43	0.33±0.08	1.44 ^{+0.22} _{-0.57}	–	162±22	S0/Sa
Main lens		1.42	15.60	3.23	0.123	0.6402	308±15	253±35	E/S0
Sandy	82.7±0.2	1.31±0.07	18.27	1.55	0.32±0.01	1.38 ^{+0.21} _{-0.56}	–	233±32	E
Main lens		1.52	16.87	2.55	0.285	0.5753	343±32	305±42	Sa/S
Rizzo	106.0±0.2	1.24±0.06	19.47	0.46	0.41±0.03	1.12 ^{+0.12} _{-0.37}	–	279±39	E
Main lens		1.68	16.43	1.95	0.158	0.7353	211±12	247±34	undetermined

Notes: F814W magnitudes are not corrected for Galactic Extinction. Uncertainties are typically 0.03 on F814W total magnitudes, 5% on R_e , and 2% on SLACS Einstein Radii (Bolton et al. 2008a).

that our procedure is unbiased and that the scatter is consistent with the estimated error bars. The latter figure shows the posterior probability distribution function for the source redshifts of the newly discovered lenses. As expected, the posterior is asymmetric with a tail to high- z due to the strong dependency on the ratio of angular diameter distances on the source redshift, when it approaches the lens redshift.

The estimated stellar velocity dispersions and source redshifts are given in Table 6. We include the spectroscopically measured σ_* when available, for comparison.

6. DISCUSSION

We begin this section by summarizing the arguments that led to our classification of the five newly discovered lens systems in Section 6.1. We then discuss the environments in which the lenses are found in Section 6.2, and in Section 6.3 we compare the properties of the new systems to the SLACS main lenses.

6.1. Validity and Properties of Candidates

Our final classification is entirely imaging-based (except in Frenchie’s case, where an SDSS spectrum was available). We thus rely entirely on lens geometry, the appearance of the subtraction residuals, and the robot’s ability to model the lens light. For this reason our standards are high: we require clearly-identified multiple images in all cases, and a straightforwardly-modeled image configuration. When available, colors are used to strengthen the case. As an additional sanity check, we note that the Einstein Radii are consistent with those expected from the FP and a simple SIE model, for sensible values of source redshifts (see Table 6). We now discuss each case individually.

Danny’s lensing galaxy is a large red elliptical, while the lensed source is blue, as expected for lens systems. The identified quad geometry is a typical lens geometry and may be called “cusp dominated” (e.g. Kochanek 2006), as it occurs when the source lies near to a cusp of the inner caustic. Although we also noted a strong disk component remaining after the initial Moffat profile subtraction, the robot is able to effectively model Danny as an SIS+external shear (a situation in which such a geometry would occur).

Sandy has two strong arcs on either side of the lens galaxy, consistent with a double pattern produced by a

source almost directly behind a SIS; this is well modeled by the robot. We note a fainter peak in surface brightness above the lens galaxy; with no obvious counter image, we believe this object is likely a small satellite galaxy in the lens plane.

The two images comprising Kenickie’s lensing event, and the center of the lensing galaxy, are not all perfectly aligned: this suggests that either the source does not lie quite on the optical axis of an ellipsoidal lens or that external shear is present. We note that the inner image appears to have more curvature than the outer; this could be brought about by unsubtracted lens-plane structure that a color image would rule out.

Frenchie, another double, has been imaged in two filters and has colors consistent with lensing. This is the only one of our systems backed by spectroscopic data. We find a spectroscopic redshift of $z_d = 0.104$. Also, a stellar velocity dispersion is available from SDSS, corresponding to $\sigma_* = 248 \pm 17$ km s⁻¹ after aperture correction, in good agreement with the value estimated via the FP technique (226 ± 27 km s⁻¹)

Rizzo is able to be modeled as a double; however the morphologies of the two identifiable images are not as well-matched as in the previous 4 cases. In the lensing scenario, the source would lie only partly within the outer caustic of the lens, with the more extended outer image being only partially strongly-lensed.

6.2. Lens environments

We expect lenses, as massive galaxies, to be clustered. Consistent with this hypothesis, 3/4 new lenses are found at redshifts very similar to those of the main SLACS lens in the field. In this section we study the environment of the fields with more than one lens to identify possible large scale structures, using the environment measures of local and global density as defined in SLACS-VIII.

SLACS-VIII found no significant difference between the environment of SLACS lenses and that of non-lensing, but otherwise identical, galaxies. With the exception of Frenchie, the environments of the newly discovered lenses are fairly typical of the overall distribution of SLACS lens environments, with the field of Kenickie being slightly under-dense, while that of Sandy being somewhat over-dense. Frenchie, as previously mentioned, lies in a very over-dense environment, the densest of all SLACS fields.

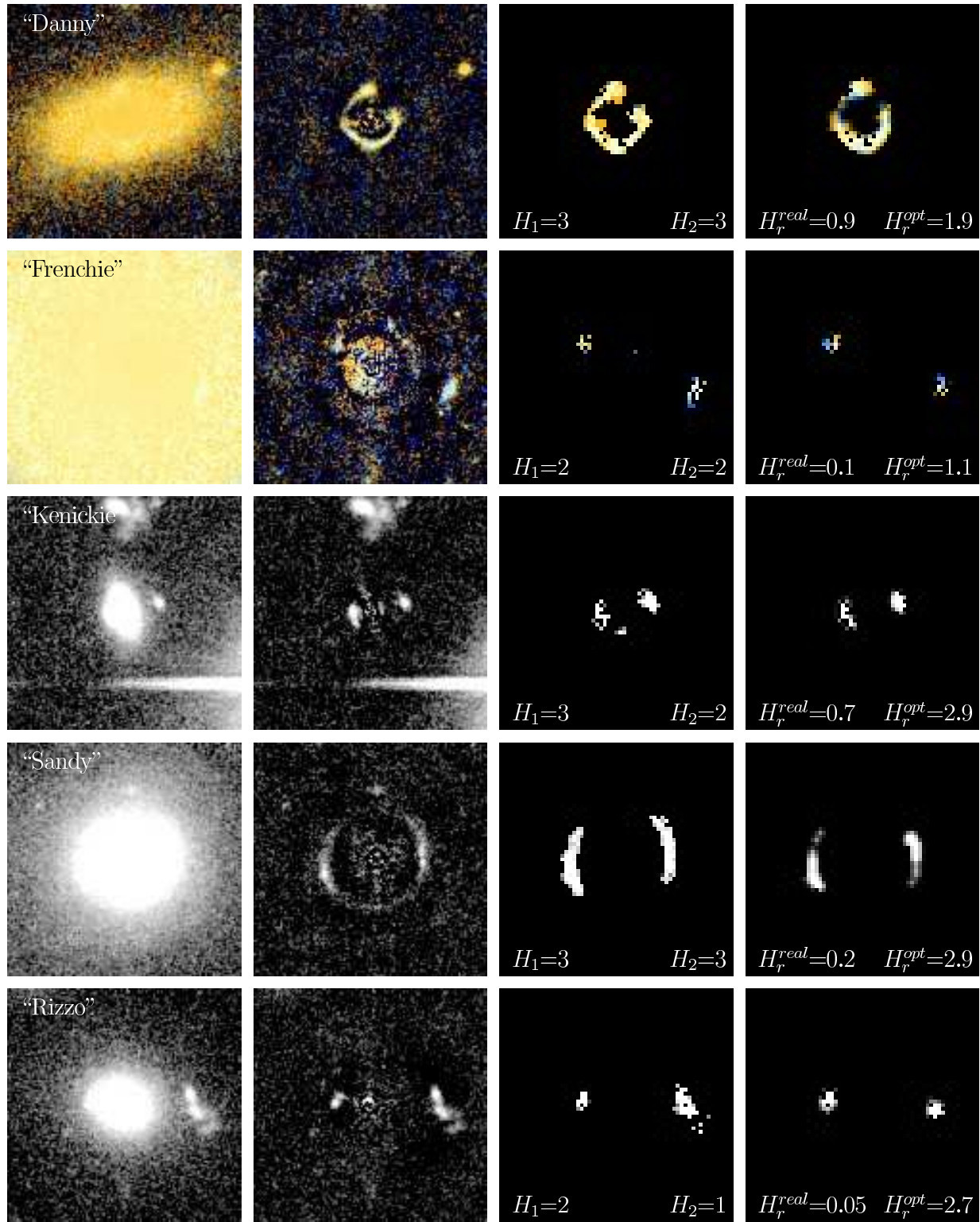


FIG. 3.— Lenses and lens models for new systems created by the HAGGLEs robot. We show the galaxy cutout (column 1), the subtraction residual (column 2), the masked robot input image (column 3), and the reconstructed images from the minimum source required to produce the configuration (column 4). The robot uses Moffat profile subtractions by default; here we have improved upon this by using a B-spline subtraction (Bolton et al. 2006). Cutouts are 6 arcseconds on a side.

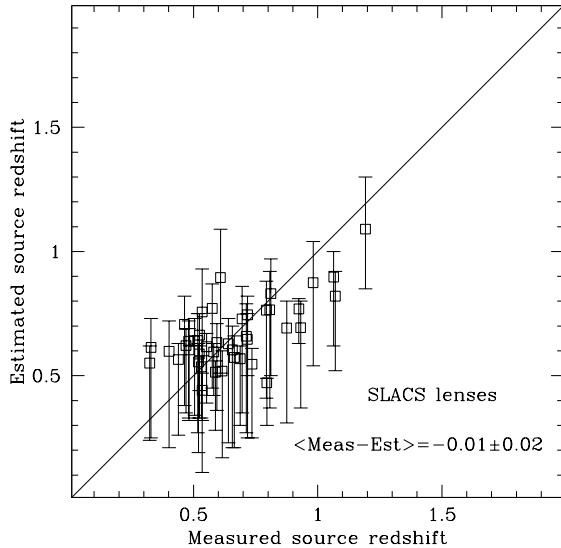


FIG. 4.— Source redshift estimated from the FP method vs. the corresponding spectroscopic source redshifts for the SLACS lenses.

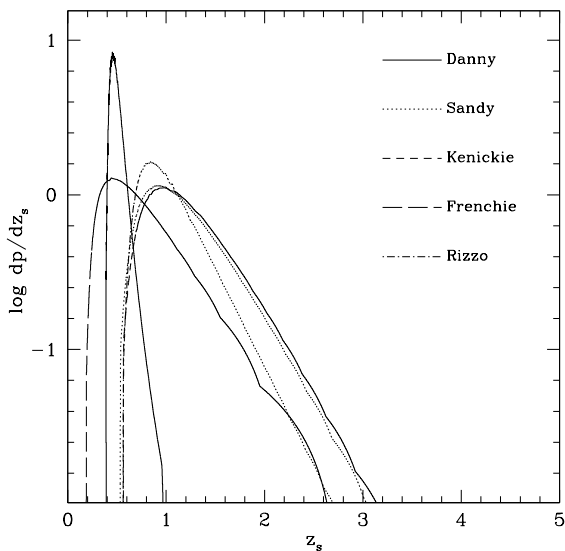


FIG. 5.— Source redshift posterior probability distribution function estimated for the newly discovered lenses using the FP method.

In fact, both Frenchie and Sandy appear associated with known clusters. Frenchie lies within SDSS-C41035, at redshift 0.106, which places both Frenchie ($z_d = 0.104$) and its main lens ($z_d = 0.106$) as members. The cluster in Sandy’s field, MaxBCGJ217.49493+41.10435, is at redshift 0.270, and the main lens at $z_d = 0.285$ lies within the cluster. We have only photometric redshift for Sandy ($z_d = 0.32 \pm 0.01$), which places it slightly beyond the extent of the cluster; however given the possible systematic errors in the photometric redshift we deem it likely that Sandy is also a member of the field’s cluster.

In conclusion, the results suggest that lens fields associate with galaxy over-densities are the most likely to present additional strong lens phenomena. Only $12/70 = 17\%$ of all SLACS lenses are associated with

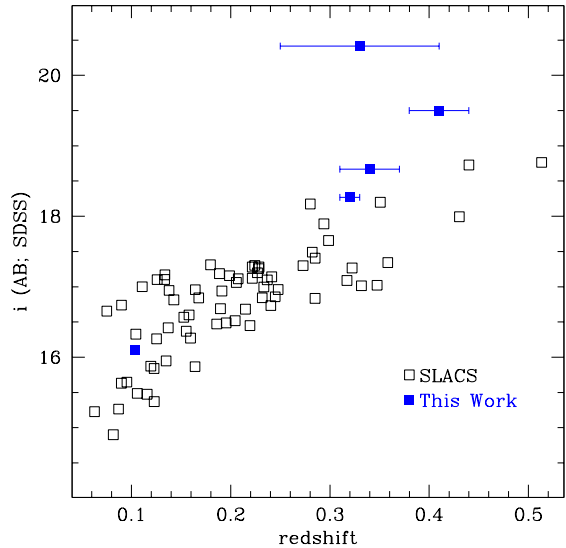


FIG. 6.— Plot of apparent i -band magnitude vs. lens redshift for the SLACS main lenses and new systems. We find that four of the five new systems are less luminous than the main lenses.

known clusters, but 50% of the newly discovered ones are (2/5 when including the likely candidate). With the present data it is hard to disentangle the contribution to the boost in strong lens surface density by the enhanced surface density of deflectors.

6.3. Comparison to SLACS lenses

We anticipated discovering lensing events similar to, but fainter than, the SLACS main lenses; we find this to be largely true. In Figure 6, we plot apparent i' magnitude against redshift for the main lenses and new systems. We find that four of the new systems are less luminous than the SLACS lenses at the same redshift, but that Frenchie is comparable. We show the distribution of stellar velocity dispersions in Figure 7; new systems are shaded.

To interpret these histograms we need to take into account the redshift dependence of the properties of the SLACS main sample. At the lower redshifts, the sample is dominated by the more abundant, slightly less massive galaxies. At higher redshifts, the flux limit of the SDSS spectroscopic database leaves only the most massive galaxies. Keeping this in mind, we also plot the distributions for the SLACS sample in the same redshift range of all the new lenses save Frenchie (> 0.26 is chosen because of a natural break in the redshift distribution; the choice of threshold does not influence our conclusions). Indeed, the newly identified lenses are less massive than the SLACS main lenses when both samples are restricted to $z_d > 0.26$. The average σ_* for the two samples are respectively $243 \pm 35 \text{ km s}^{-1}$ and $299 \pm 20 \text{ km s}^{-1}$.

6.4. Lens abundance

In Table 8, we compare lensing rates (or abundances, in degree^{-2}) for four HST imaging surveys, including this one. The quoted uncertainties on the inferred rates delimit the Bayesian 68% confidence interval, assuming Poisson statistics and a uniform prior PDF. As noted

TABLE 7
ENVIRONMENTS OF NEW LENSES AND CANDIDATES

Short name	SDSS field	local overdensity	global overdensity	Cluster	z_{Cl}
Danny	J0737+3216	1.55 ± 0.50	1.22 ± 0.28	None	
Frenchie	J1143-0144	79 ± 25.5	3.7 ± 0.50	SDSS-C41035	0.106
Kenickie	J1213+6708	0.48 ± 0.16	0.45 ± 0.16	None	
Sandy	J1430+4105	1.83 ± 0.62	1.22 ± 0.34	MaxBCGJ217.49493+41.10435	0.270
Rizzo	J1103+5322	0.98 ± 0.3	0.75 ± 0.18	None	

previously, classification systems across surveys are not consistent, thus one must impose similar criteria when comparing the results of different surveys; naturally there will be differences in opinion. In this work we do not rely on spectroscopic data to classify a lens as “definite” and instead require that lens morphology, surface brightness, and color (if available) are clearly identifiable with a typical lens geometry. Due to the limited data available, we apply these criteria rigorously. With the goal of applying similar criteria to all surveys considered, we take as definite lenses: the literature-confirmed lenses for MDS, the “unambiguous” candidates for AEGIS, the “best” candidates for COSMOS, and the $H = 3$ lenses for this work.

The largest survey of “blank” sky undertaken to date is the COSMOS survey (Faure et al. 2008), whose findings imply a measured lensing rate of around 12 lenses per square degree. Since our data are of comparable depth (and in the same single filter), we adopt this as our fiducial value. Given this lensing rate, we might expect to find 1.61 lenses, instead of our observed 4. Assuming a uniform prior on the lensing rate we find that the inferred lensing rate from our survey is 30^{+24}_{-8} lenses/degree².

The uniform prior is somewhat unrealistic – it does not down-weight the occasional high lens yields that could arise as statistical flukes from the long-tailed Poisson likelihood. A maximally conservative approach would be to take the COSMOS rate as the mean of an exponential prior; in this case, we infer a lensing rate of 18^{+14}_{-5} lenses/degree². We still find a significantly higher lens abundance than seen in the COSMOS survey: with the COSMOS prior the probability that the lensing rate in the SLACS fields is greater than 12 degree⁻² is 88%. Relaxing the assumption that our fields are similar in nature to those in COSMOS and reverting to the uniform prior, we find that there is only a $\sim 2\%$ chance that the lensing rate in the SLACS fields is less than the COSMOS rate of 12 lenses/degree².

Although no definitive conclusions can be drawn due to the small numbers and variety of surveys, the results from this project do support the hypothesis of Fassnacht et al. (2006) that looking near known lenses increases the efficiency of finding new lenses.

7. CONCLUSIONS

We have performed a highly efficient search for gravitational lenses based purely on imaging data. Our search area consisted of 44 HST/ ACS fields, each centered on a SLACS “definite” lens, therefore exploiting the expected clustering of gravitational lenses in each field. We compared the purity, completeness, and investigator time for four different search methods. These methods are comprised of: (1) use of the output from the HAGGLEs robot, (2) inspection of BG subtraction residual images, (3) inspection of BG cutout images, (4) full frame visual

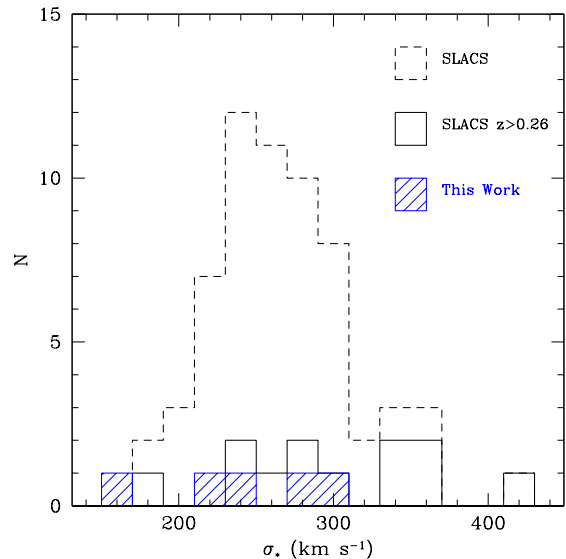


FIG. 7.— Histogram of central velocity dispersions for main lenses and new systems; new systems are shaded. Main lens velocity dispersion were aperture-corrected from SDSS photometry, while we used the FP relation to calculate the values for new lenses.

TABLE 8
LENSING RATES FOR SELECTED SURVEYS

Survey	Area (deg ²)	N_{lenses}	Lensing rate (degree ⁻²)
MDS ¹	0.17	2	12^{+15}_{-3}
AEGIS ²	0.19	3	16^{+15}_{-5}
COSMOS ³	1.64	20	12^{+4}_{-2}
This Work	0.13	4	31^{+24}_{-9}
with COSMOS prior		(predicts 1.6)	18^{+14}_{-5}

Confidence intervals are Bayesian 68%, assuming Poisson statistics and a uniform prior on the lensing rate, except in the final row where the COSMOS rate is taken as the mean of an exponential prior. Relevant citations are as follows: ¹ Ratnatunga et al. (1999), ² Moustakas et al. (2007), ³ Faure et al. (2008)

inspection of ACS fields.

Our main conclusions are:

- Taking into account efficiency as well as completeness and purity, we find that of the methods used, procedures 1 (using output from the HAGGLEs robot) and 2 (looking at subtraction residuals of bright galaxies) have the best performance. In situations where the simple SIS+external shear model used by the robot may be insufficient – such as in clusters or to find naked cusp configurations – it may be most effective to use a combination of procedures 1 and 2, in order to inspect all objects modeled by the robot. However, looking at only

the bright galaxies (BGs) in the fields did not decrease the completeness of this particular survey, while doing so greatly improved efficiency.

- We discovered four new strong lenses and one promising candidate in the course of our survey. We find that 3/4 of these new lens systems have lens redshifts similar to those of their main lenses; additionally, two of the new lenses are found in clusters of galaxies that also include their respective main lenses.
- We find that 3/4 new systems are less luminous and less massive than the SLACS lenses. Overall, we are probing early-type galaxies at higher redshifts and lower masses than the SLACS survey. For these comparisons, we used the data from the improved robot models, available photometry, and the Fundamental Plane to estimate the central velocity dispersions and source redshifts for each of our new systems.
- The lens abundance for this survey, 30_{-8}^{+24} lenses/degree² (uniform prior), is markedly higher than the lensing rates for the three other HST surveys considered at comparable depths and resolution. Despite the small numbers and variations in search methods, this result supports the idea that searching near known lenses increases the yield of a lens survey.

The HAGGLEs project is currently using a combination of procedures 1 and 2 to search for new lenses in the HST archive; through efforts such as this and others, we will be able to refine our lens search techniques for future surveys covering much larger areas of the sky. The use of efficient and repeatable lens search methods will further us towards the goal of having a large, homogenous sample of strong gravitational lenses. Such a sample will enable us to calculate a lens-lens correlation function and constrain the statistical properties of halos containing lens galaxies.

This paper builds on the work of the SLACS and HAGGLES collaborations. We are grateful to our SLACS and HAGGLES collaborators and friends – Adam Bolton, Roger Blandford, Maruša Bradač, Scott Burles, Chris Fassnacht, Raphaël Gavazzi, David Hogg, Leon Koopmans, Leonidas Moustakas, Eric Morganson, and Tim Schrabback-Krahe – for their many insightful comments and suggestions throughout this project. Support for HST programs #10174, #10587, #10886, #10676, #10494, and #10798 was provided by NASA through a grant from the Space Telescope Science Institute, which is operated by the Association of Universities for Research in Astronomy, Inc., under NASA contract NAS 5-26555. E.R.N. acknowledges partial financial support from the College of Creative Studies. The work of P.J.M. was supported by the TABASGO foundation in the form of a research fellowship. T.T. acknowledges support from the NSF through CAREER award NSF-0642621, by the Sloan Foundation through a Sloan Research Fellowship, and by the Packard Foundation through a Packard Fellowship. This research has made use of the NASA/IPAC

Extragalactic Database (NED) which is operated by the Jet Propulsion Laboratory, California Institute of Technology, under contract with the National Aeronautics and Space Administration. This project would not have been feasible without the extensive and accurate database provided by the Digital Sloan Sky Survey (SDSS). Funding for the creation and distribution of the SDSS Archive has been provided by the Alfred P. Sloan Foundation, the Participating Institutions, the National Aeronautics and Space Administration, the National Science Foundation, the U.S. Department of Energy, the Japanese Monbukagakusho, and the Max Planck Society. The SDSS Web site is <http://www.sdss.org/>. The SDSS is managed by the Astrophysical Research Consortium (ARC) for the Participating Institutions. The Participating Institutions are The University of Chicago, Fermilab, the Institute for Advanced Study, the Japan Participation Group, The Johns Hopkins University, the Korean Scientist Group, Los Alamos National Laboratory, the Max-Planck-Institute for Astronomy (MPIA), the Max-Planck-Institute for Astrophysics (MPA), New Mexico State University, University of Pittsburgh, University of Portsmouth, Princeton University, the United States Naval Observatory, and the University of Washington.

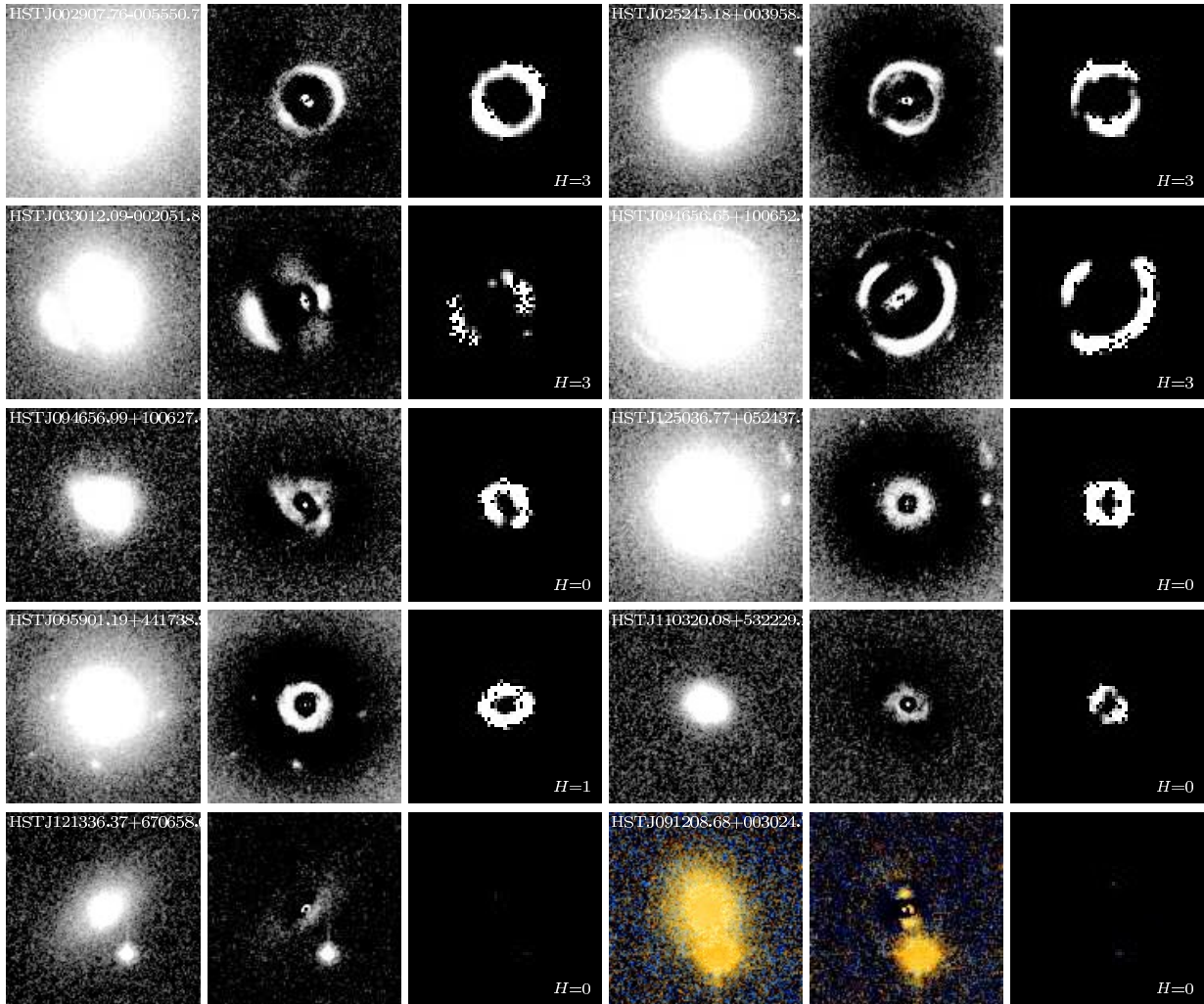


FIG. 8.— Objects classified by the robot as $H_r^{real} > 2.5$, including four main lenses (first and second rows). Cutouts are 6 arcseconds on a side. We find common false identifications to be rings left by the Moffat subtraction, unmasked disks, and nearby galaxies.

APPENDIX

SUPPLEMENTARY FIGURES AND TABLES

In this Appendix we give a more complete illustration of the HAGGLEs robot’s performance when given the SLACS main lenses. In Figure 8 we show all objects classified by the *realistic* robot as $H_r^{real} > 2.5$: Marshall et al. (2008) found this to give a sample with $\sim 20\%$ completeness but $\sim 100\%$ purity. In the SLACS fields, 10 objects were classified as $H_r^{real} > 2.5$, including 4 main lenses. Comparing to the human-classified results using the same input data (Procedure 2, Table 3), this represents a completeness of $\sim 11\%$ and a purity of 40%. Some explanation for these differences are given in the main text.

The classification of the SLACS main lenses is listed in full in Table 9. The survey cutout images of these systems, sorted into bins in H_r^{opt} , are shown in Figure 9 ($H_r^{opt} > 2.5$), Figure 10 ($1.5 < H_r^{opt} < 2.5$), and Figure 12 ($H_r^{opt} < 1.5$). For each system, we show the full cutout image as presented for inspection in Procedure 3, the lens galaxy-subtracted cutout image as presented for inspection in Procedure 2, and the lensed images and counter-images predicted by the HAGGLEs robot’s best lens model.

REFERENCES

- Alard, C. 2006, ArXiv Astrophysics e-prints
 Belokurov, V., Evans, N. W., Moiseev, A., King, L. J., Hewett, P. C., Pettini, M., Wyrzykowski, L., McMahon, R. G., Smith, M. C., Gilmore, G., Sanchez, S. F., Udalski, A., Kozlov, S., Zucker, D. B., & Walcher, C. J. 2007, ApJ, 671, L9
 Bolton, A. S., Burles, S., Koopmans, L. V. E., Treu, T., Gavazzi, R., Moustakas, L. A., Wayth, R., & Schlegel, D. J. 2008a, ApJ, 682, 964
 Bolton, A. S., Burles, S., Koopmans, L. V. E., Treu, T., & Moustakas, L. A. 2006, ApJ, 638, 703
 Bolton, A. S., Treu, T., Koopmans, L. V. E., Gavazzi, R., Moustakas, L. A., Burles, S., Schlegel, D. J., & Wayth, R. 2008b, ArXiv e-prints, 805

TABLE 9
CLASSIFICATION OF SLACS MAIN LENSES BY METHOD

Object name	H_1	H_2	H_3	H_4	H_r^{opt}	H_r^{real}	Additional ACS filters
SDSSJ0008-0004	2	2	2	3	2.9	0.7	–
SDSSJ0029-0055	3	3	0	3	2.9	2.8	–
SDSSJ0157-0056	0	3	1	3	1.3	0.0	–
SDSSJ0216-0813	3	3	0	3	2.0	1.9	–
SDSSJ0252+0039	3	3	0	3	2.9	2.7	–
SDSSJ0330-0020	3	3	2	3	2.9	2.8	–
SDSSJ0728+3835	3	3	0	3	1.9	1.9	–
SDSSJ0737+3216	3	3	3	3	2.9	2.4	F555W
SDSSJ0808+4706	3	3	0	3	1.9	0.9	–
SDSSJ0822+2652	3	3	0	3	2.4	1.9	–
SDSSJ0841+3824	2	2	0	3	2.0	1.3	–
SDSSJ0903+4116	3	3	1	3	1.9	1.7	–
SDSSJ0912+0029	3	3	0	2	1.8	0.1	F555W
SDSSJ0936+0913	3	3	0	2	1.9	1.3	–
SDSSJ0946+1006	3	3	2	3	2.9	2.8	–
SDSSJ0956+5100	0	3	1	3	0	0	F555W
SDSSJ0959+0410	3	3	1	3	2.0	1.9	F555W
SDSSJ0959+4416	2	1	0	3	2.9	0.7	–
SDSSJ1016+3859	0	1	1	2	1.0	0.0	–
SDSSJ1020+1122	3	3	1	2	1.5	0.8	–
SDSSJ1023+4230	3	3	0	3	1.9	1.7	–
SDSSJ1029+0420	0	1	0	1	0	0	–
SDSSJ1032+5322	0	1	0	1	1.4	0.2	–
SDSSJ1103+5322	0	3	0	3	0	0	–
SDSSJ1142+1001	2	2	0	2	1.9	1.9	–
SDSSJ1143-0144	3	3	2	3	1.9	0.5	F555W
SDSSJ1153+4612	3	3	0	3	1.7	1.0	–
SDSSJ1205+4910	3	3	3	3	1.9	1.9	F555W
SDSSJ1213+6708	1	1	0	3	2.3	1.9	–
SDSSJ1218+0830	3	3	0	3	2.9	0.7	–
SDSSJ1250+0523	3	3	0	3	1.9	1.9	–
SDSSJ1402+6321	3	3	0	3	1.6	0.4	F555W
SDSSJ1416+5136	0	3	0	3	0	0	–
SDSSJ1420+6019	3	3	0	3	2.1	0.1	–
SDSSJ1430+4105	3	3	1	3	1.9	1.7	–
SDSSJ1432+6317	3	2	0	3	2.9	2.1	–
SDSSJ1451-0239	0	3	2	3	0	0	F555W
SDSSJ1525+3327	2	2	0	2	2.0	1.9	–
SDSSJ1627-0053	3	3	2	3	2.9	2.1	F555W
SDSSJ1630+4520	3	3	1	3	1.9	0.2	F555W
SDSSJ2238-0754	3	3	1	3	2.2	0.0	F555W
SDSSJ2300+0022	3	3	0	3	1.8	0.0	F555W
SDSSJ2303+1422	3	3	0	3	1.8	0.0	F555W
SDSSJ2341+0000	3	3	0	3	2.2	1.7	–

Note: $H_1 = 0$ indicates that the system was not inspected; these objects have $H_r^{opt} < 1.5$

Browne, I. W. A., Wilkinson, P. N., Jackson, N. J. F., Myers, S. T., Fassnacht, C. D., Koopmans, L. V. E., Marlow, D. R., Norbury, M., Rusin, D., Sykes, C. M., Biggs, A. D., Blandford, R. D., de Bruyn, A. G., Chae, K.-H., Helbig, P., King, L. J., McKean, J. P., Pearson, T. J., Phillips, P. M., Readhead, A. C. S., Xanthopoulos, E., & York, T. 2003, MNRAS, 341, 13
Cabanac, R. A., Alard, C., Dantel-Fort, M., Fort, B., Gavazzi, R., Gomez, P., Kneib, J. P., Le Fèvre, O., Mellier, Y., Pello, R., Soucail, G., Sygnet, J. F., & Valls-Gabaud, D. 2007, A&A, 461, 813
Djorgovski, S., & Davis, M. 1987, ApJ, 313, 59
Dressler, A., Lynden-Bell, D., Burstein, D., Davies, R. L., Faber, S. M., Terlevich, R., & Wegner, G. 1987, ApJ, 313, 42
Estrada, J., Annis, J., Diehl, H. T., Hall, P. B., Las, T., Lin, H., Makler, M., Merritt, K. W., Scarpine, V., Allam, S., & Tucker, D. 2007, ApJ, 660, 1176

Fassnacht, C. D., McKean, J. P., Koopmans, L. V. E., Treu, T., Blandford, R. D., Auger, M. W., Jeltama, T. E., Lubin, L. M., Margoniner, V. E., & Wittman, D. 2006, ApJ, 651, 667
Fassnacht, C. D., Moustakas, L. A., Casertano, S., Ferguson, H. C., Lucas, R. A., & Park, Y. 2004, ApJ, 600, L155
Faure, C., Kneib, J.-P., Covone, G., Tasca, L., Leauthaud, A., Capak, P., Jahnke, K., Smolcic, V., de la Torre, S., Ellis, R., Finoguenov, A., Koekemoer, A., Le Fèvre, O., Massey, R., Mellier, Y., Refregier, A., Rhodes, J., Scoville, N., Schinnerer, E., Taylor, J., Van Waerbeke, L., & Walcher, J. 2008, ApJS, 176, 19
Gavazzi, R., Treu, T., Koopmans, L. V. E., Bolton, A. S., Moustakas, L. A., Burles, S., & Marshall, P. J. 2008, ArXiv e-prints, 801
Gavazzi, R., Treu, T., Rhodes, J. D., Koopmans, L. V., Bolton, A. S., Burles, S., Massey, R., & Moustakas, L. A. 2007, ArXiv Astrophysics e-prints

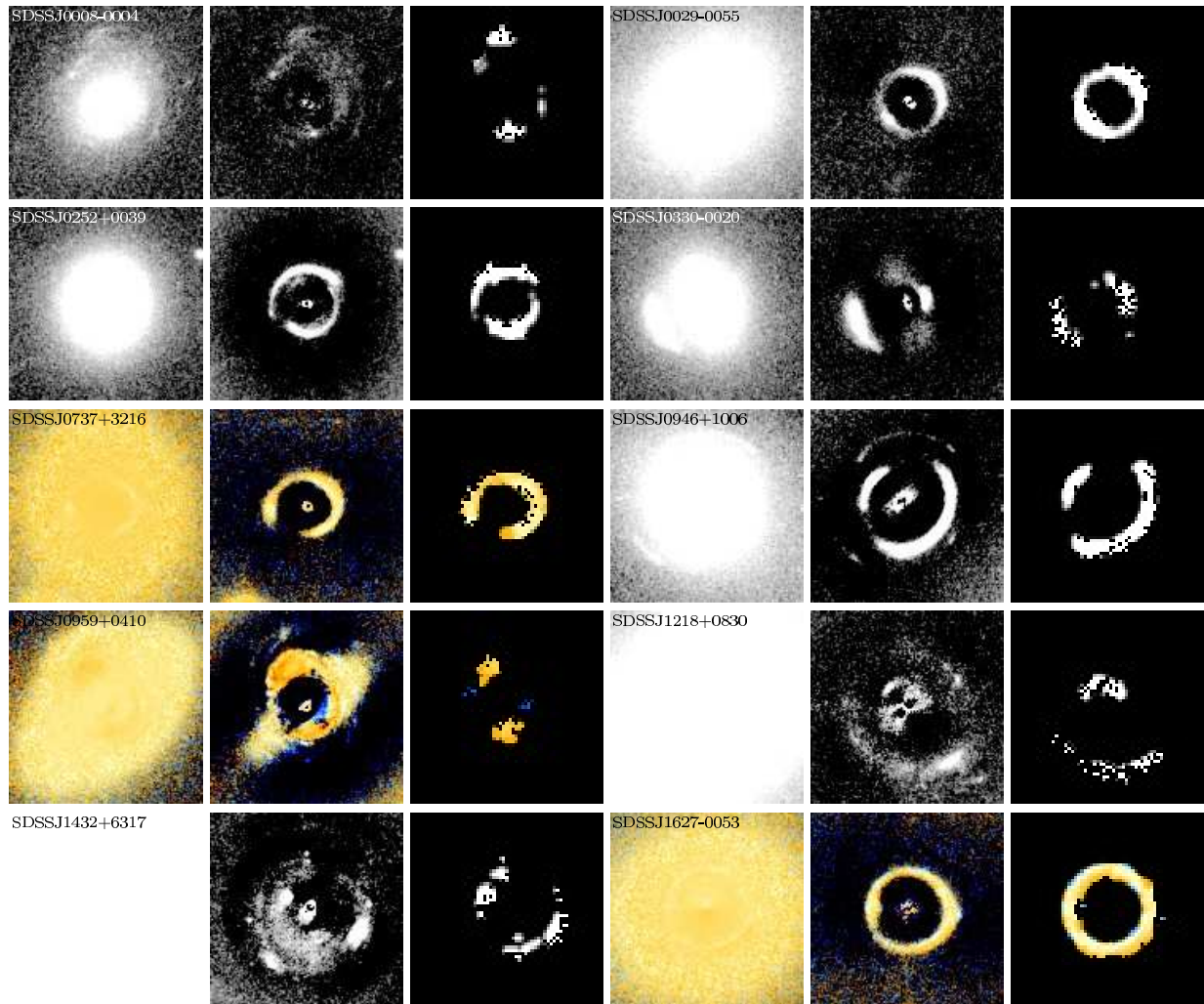


FIG. 9.— Robot output for SLACS main lenses with $H_r^{opt} > 2.5$, including: galaxy cutouts (col. 1,4), residuals after Moffat subtraction (col. 2,5), and predicted images from the robot lens models (col. 3,6). In this figure and the two following, cutouts are 6 arcsec on a side.

- Inada, N., Oguri, M., Becker, R. H., Shin, M.-S., Richards, G. T., Hennawi, J. F., White, R. L., Pindor, B., Strauss, M. A., Kochanek, C. S., Johnston, D. E., Gregg, M. D., Kayo, I., Eisenstein, D., Hall, P. B., Castander, F. J., Clocchiatti, A., Anderson, S. F., Schneider, D. P., York, D. G., Lupton, R., Chiu, K., Kawano, Y., Scranton, R., Frieman, J. A., Keeton, C. R., Morokuma, T., Rix, H.-W., Turner, E. L., Burles, S., Brunner, R. J., Sheldon, E. S., Bahcall, N. A., & Masataka, F. 2008, *AJ*, 135, 496
- Jackson, N. 2008, *ArXiv e-prints*, 806
- Kochanek, C. S. 2006, in *Gravitational Lensing: Strong, Weak & Micro*, ed. G. Meylan, P. Jetzer, & P. North, *Lecture Notes of the 33rd Saas-Fee Advanced Course* (Springer-Verlag: Berlin)
- Koopmans, L. V. E., Treu, T., Bolton, A. S., Burles, S., & Moustakas, L. A. 2006, *ApJ*, 649, 599
- Kubo, J. M., & Dell'Antonio, I. P. 2008, *MNRAS*, 385, 918
- Maiz, D., Rix, H.-W., Gal-Yam, A., & Gould, A. 1997, *ApJ*, 486, 75
- Marshall, P., Blandford, R., & Sako, M. 2005, *New Astronomy Review*, 49, 387
- Marshall, P. J., Hogg, D. W., Moustakas, L. A., Fassnacht, C. D., Bradac, M., Schrabback, T., & Blandford, R. D. 2008, *ArXiv e-prints*, 805
- Moustakas, L. A., Marshall, P., Newman, J. A., Coil, A. L., Cooper, M. C., Davis, M., Fassnacht, C. D., Guhathakurta, P., Hopkins, A., Koekemoer, A., Konidaris, N. P., Lotz, J. M., & Willmer, C. N. A. 2007, *ApJ*, 660, L31
- Myers, S. T., Jackson, N. J., Browne, I. W. A., de Bruyn, A. G., Pearson, T. J., Readhead, A. C. S., Wilkinson, P. N., Biggs, A. D., Blandford, R. D., Fassnacht, C. D., Koopmans, L. V. E., Marlow, D. R., McKean, J. P., Norbury, M. A., Phillips, P. M., Rusin, D., Shepherd, M. C., & Sykes, C. M. 2003, *MNRAS*, 341, 1
- Oguri, M., Inada, N., Pindor, B., Strauss, M. A., Richards, G. T., Hennawi, J. F., Turner, E. L., Lupton, R. H., Schneider, D. P., Fukugita, M., & Brinkmann, J. 2006, *AJ*, 132, 999
- Peng, C. Y., Ho, L. C., Impey, C. D., & Rix, H.-W. 2002, *AJ*, 124, 266
- Pindor, B., Turner, E. L., Lupton, R. H., & Brinkmann, J. 2003, *AJ*, 125, 2325
- Ratnatunga, K. U., Griffiths, R. E., & Ostrander, E. J. 1999, *AJ*, 117, 2010
- Seidel, G., & Bartelmann, M. 2007, *A&A*, 472, 341
- Treu, T., Gavazzi, R., Gorecki, A., Marshall, P. J., Koopmans, L. V. E., Bolton, A. S., Moustakas, L. A., & Burles, S. 2008, *ApJ*, in press, 806
- Treu, T., Koopmans, L. V., Bolton, A. S., Burles, S., & Moustakas, L. A. 2006, *ApJ*, 640, 662
- Treu, T., Stiavelli, M., Möller, P., Casertano, S., & Bertin, G. 2001, *MNRAS*, 326, 221
- Turner, E. L., Ostriker, J. P., & Gott, III, J. R. 1984, *ApJ*, 284, 1

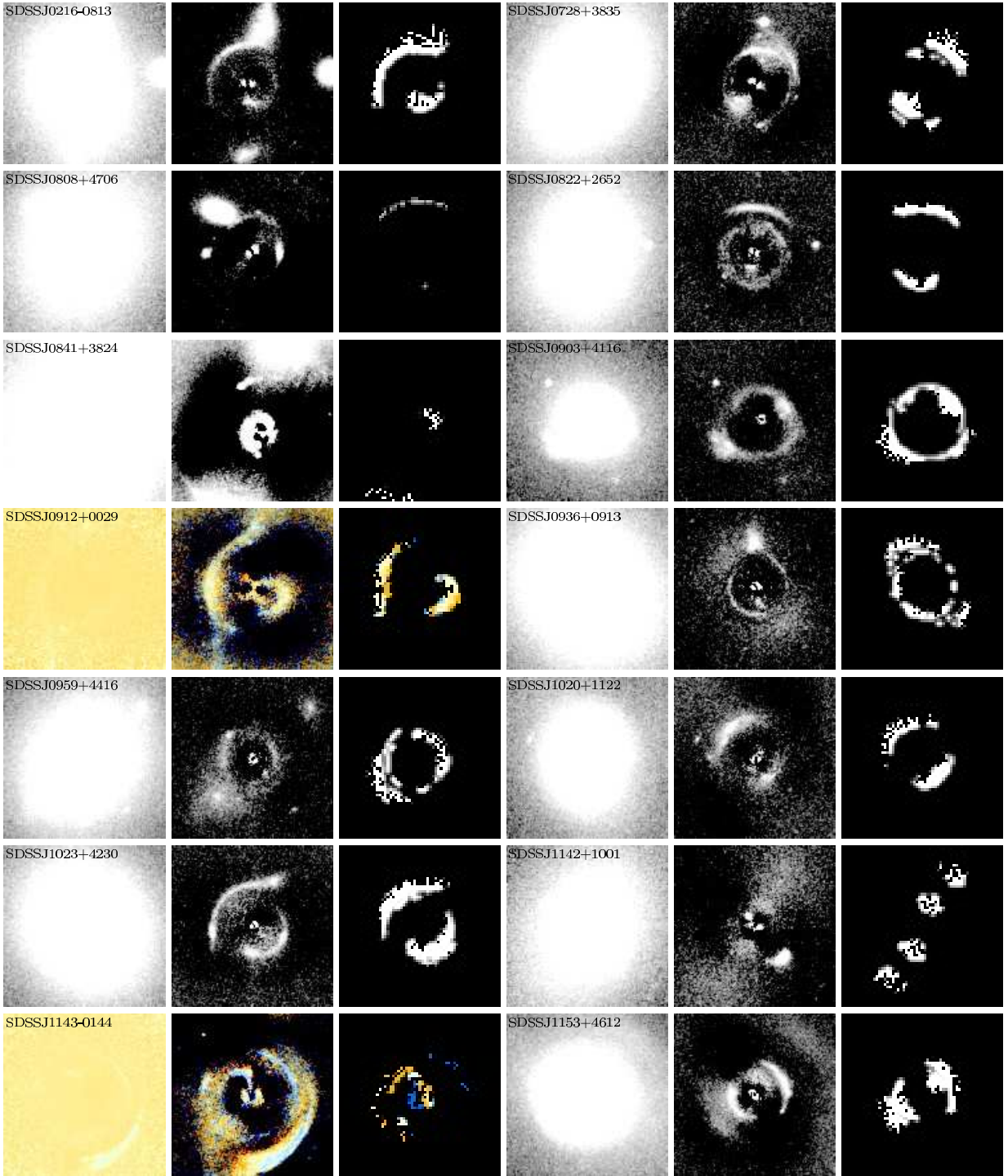


FIG. 10.— Robot output for SLACS main lenses with $1.5 < H_r^{opt} < 2.5$, including galaxy cutouts, subtraction residuals, and predicted images from the robot lens models.

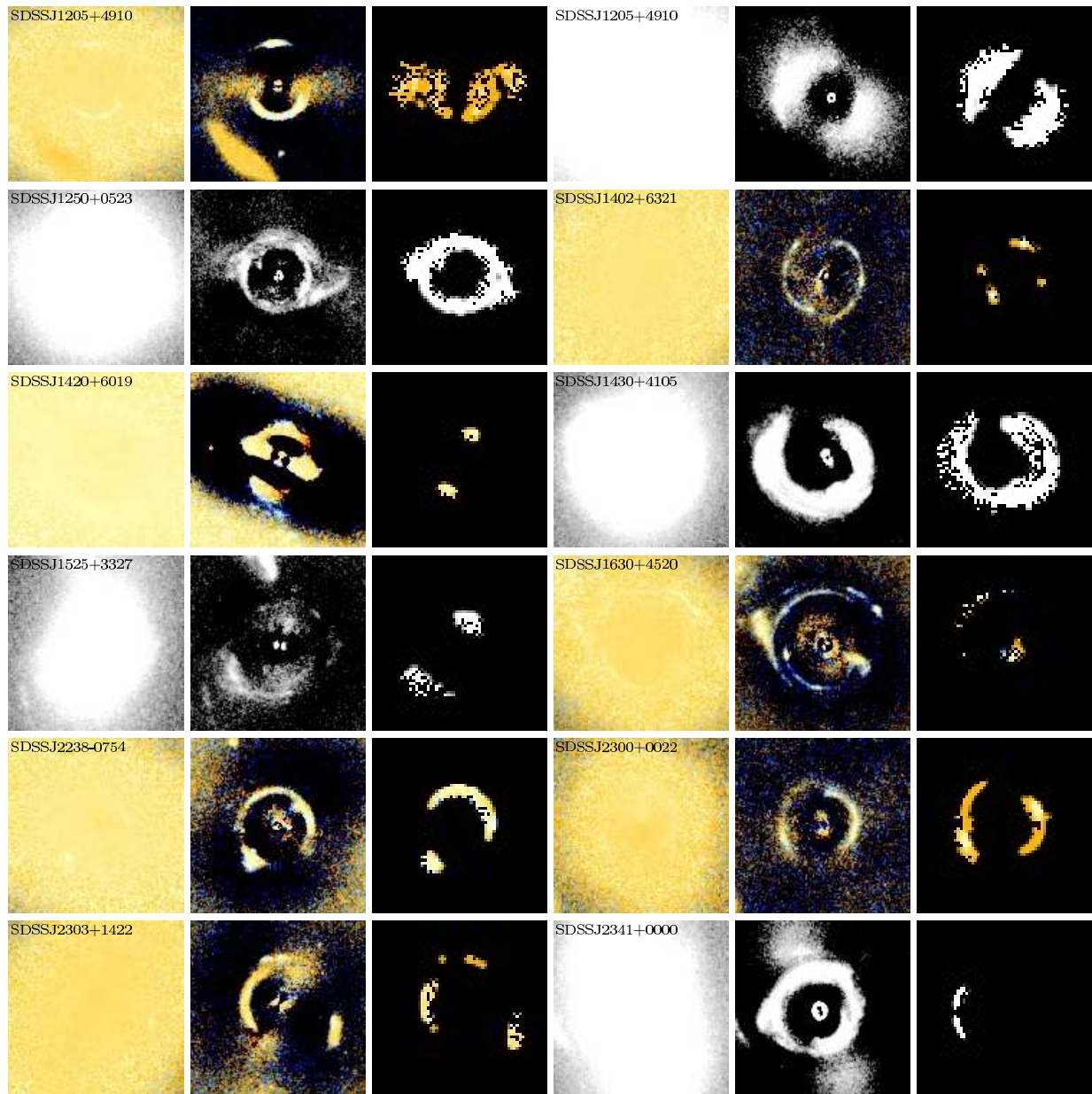


FIG. 11.— Continuation of Figure 10.

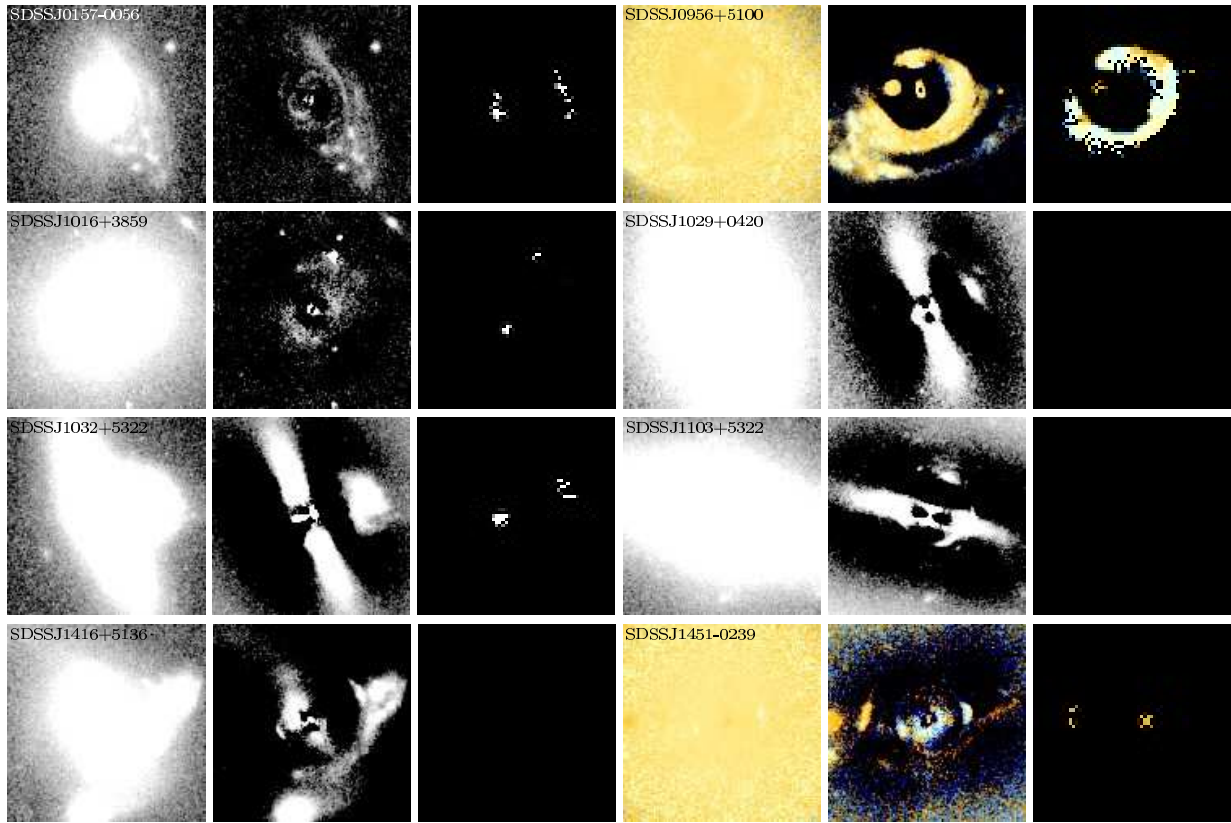


FIG. 12.— Robot output for SLACS main lenses with $H_r^{opt} < 1.5$, including galaxy cutouts, subtraction residuals, and predicted images from the robot lens models.